Robust Circadian Oscillations in Growing Cyanobacteria Require Transcriptional Feedback

Shu-Wen Teng *et al.*

Science **340**, 737 (2013);
DOI: 10.1126/science.1230996

Science (print ISSN 0036-8075; online ISSN 1095-9203) is published weekly, except the last week in December, by the American Association for the Advancement of Science, 1200 New York Avenue NW, Washington, DC 20005.

the predicted behavior of the atomic collapse state having lowest angular momentum ($j = 1/2$) and lowest energy (*8*, *9*). In principle, an infinite number of resonances (corresponding to different principle quantum numbers) should appear in the supercritical regime. However, because their energies follow an exponential sequence and their spatial extent is inversely proportional to their energy measured from the Dirac point (*8*, *9*), only the lowest energy state should be detectable within our experimental resolution (screening suppresses all states with sufficiently large spatial extent).

The strong doping dependence of the intensity of the atomic collapse state (Fig. 3) can be partially explained as a screening effect. In the p-doped regime, the atomic collapse state is experimentally observed to shift to lower energy with respect to the Dirac point for decreased p-doping. This can be explained by free-electron–like screening (*23*, *24*), because reduced screening should result in an increase of the effective charge of the artificial nucleus. The n-doped regime, however, shows a completely different behavior. Here, the amplitude of the atomic collapse state essentially disappears as it moves beneath E_F (i.e., as it becomes occupied with charge carriers). We believe that this behavior arises from internal correlation among the quasi-localized charge carriers that inhabit the atomic collapse state (only one out of the four electron states allowed due to spin and valley degeneracy can be occupied at any given time) (*25*). Interaction between these electrons reduces the single-particle spectral function as measured in scanning tunneling spectroscopy, but the precise mechanism for this reduction remains to be determined.

References and Notes

1. W. Greiner, B. Muller, J. Rafelski, *Quantum Electrodynamics of Strong Fields* (Springer, Berlin, 1985).
2. I. Pomeranchuk, Y. Smorodinsky, *J. Phys. USSR* **9**, 97 (1945).
3. Y. B. Zeldovich, V. S. Popov, *Sov. Phys. Usp.* **14**, 673 (1972).
4. C. G. Darwin, *Philos. Mag. Ser. 6* **25**, 201 (1913).
5. T. H. Boyer, *Am. J. Phys.* **72**, 992 (2004).
6. T. Cowan *et al.*, *Phys. Rev. Lett.* **54**, 1761 (1985).
7. J. Schweppe *et al.*, *Phys. Rev. Lett.* **51**, 2261 (1983).
8. V. M. Pereira, J. Nilsson, A. H. Castro Neto, *Phys. Rev. Lett.* **99**, 166802 (2007).
9. A. V. Shytov, M. I. Katsnelson, L. S. Levitov, *Phys. Rev. Lett.* **99**, 246802 (2007).
10. A. V. Shytov, M. I. Katsnelson, L. S. Levitov, *Phys. Rev. Lett.* **99**, 236801 (2007).
11. A. H. Castro Neto, F. Guinea, N. M. R. Peres, K. S. Novoselov, A. K. Geim, *Rev. Mod. Phys.* **81**, 109 (2009).
12. K. S. Novoselov *et al.*, *Nature* **438**, 197 (2005).
13. Y. Zhang, Y. W. Tan, H. L. Stormer, P. Kim, *Nature* **438**, 201 (2005).
14. Y. Wang *et al.*, *Nat. Phys.* **8**, 653 (2012).
15. X. Li *et al.*, *Science* **324**, 1312 (2009).
16. C. R. Dean *et al.*, *Nat. Nanotechnol.* **5**, 722 (2010).
17. R. Decker *et al.*, *Nano Lett.* **11**, 2291 (2011).
18. J. Xue *et al.*, *Nat. Mater.* **10**, 282 (2011).
19. Supplementary materials are available on *Science* Online.
20. Y. Zhang *et al.*, *Nat. Phys.* **4**, 627 (2008).
21. V. W. Brar *et al.*, *Phys. Rev. Lett.* **104**, 036805 (2010).
22. E. J. Heller, M. F. Crommie, C. P. Lutz, D. M. Eigler, *Nature* **369**, 464 (1994).
23. T. Ando, *Phys. Soc. Japan* **75**, 074716 (2006).
24. E. H. Hwang, S. Das Sarma, *Phys. Rev. B* **75**, 205418 (2007).
25. V. N. Kotov, B. Uchoa, V. M. Pereira, F. Guinea, A. H. Castro Neto, *Rev. Mod. Phys.* **84**, 1067 (2012).
26. J. Li, W.-D. Schneider, R. Berndt, *Phys. Rev. B* **56**, 7656 (1997).
27. C. Wittneven, R. Dombrowski, M. Morgenstern, R. Wiesendanger, *Phys. Rev. Lett.* **81**, 5616 (1998).

Acknowledgments: Our research was supported by the Office of Naval Research Multidisciplinary University Research Initiative award no. N00014-09-1-1066 (graphene device preparation, characterization, and imaging); the Director, Office of Science, Office of Basic Energy Sciences of the U.S. Department of Energy (DOE) under contract no. DE-AC02-05CH11231 (STM instrumentation development and spectroscopy); NSF award nos. EEC-0832819 (*dI/dV* simulations) and DMR10-1006184 (DFT calculations); and Engineering and Physical Sciences Research Council grant EP/G036101/1 (Dirac equation calculations). Computational resources were provided by DOE at the LBNL National Energy Research Scientific Computing Center.

Supplementary Materials

www.sciencemag.org/cgi/content/full/science.1234320/DC1
Materials and Methods
Supplementary Text
Figs. S1 to S10
References (*28*–*37*)

20 December 2012; accepted 20 February 2013
Published online 7 March 2013;
10.1126/science.1234320

Robust Circadian Oscillations in Growing Cyanobacteria Require Transcriptional Feedback

Shu-Wen Teng,[1] Shankar Mukherji,[1]* Jeffrey R. Moffitt,[2]* Sophie de Buyl,[3]* Erin K. O'Shea[1]†

The remarkably stable circadian oscillations of single cyanobacteria enable a population of growing cells to maintain synchrony for weeks. The cyanobacterial pacemaker is a posttranslational regulation (PTR) circuit that generates circadian oscillations in the phosphorylation state of the clock protein KaiC. Layered on top of the PTR is transcriptional-translational feedback regulation (TTR), common to all circadian systems, consisting of a negative feedback loop in which KaiC regulates its own production. We found that the PTR circuit is sufficient to generate oscillations in growing cyanobacteria. However, in the absence of TTR, individual oscillators were less stable and synchrony was not maintained in a population of cells. Experimentally constrained mathematical modeling reproduced sustained oscillations in the PTR circuit alone and demonstrated the importance of TTR for oscillator synchrony.

Circadian clocks are present in all forms of life and are crucial in coordinating physiology with the day and night cycle (*1*, *2*). Clocks can maintain oscillation phase, frequency, and amplitude for many cycles even in the absence of external cues (*3*). In the cyanobacterial species *Synechococcus elongatus*, circadian oscillations exhibit remarkable temporal stability with a correlation time of many weeks in constant environmental conditions (*4*, *5*).

Circadian oscillations in *S. elongatus* are generated by a network architecture that consists of two regulatory loops: (i) a posttranslational regulation (PTR) circuit whose output is circadian oscillations in the phosphorylation state of KaiC, an enzyme that catalyzes its own phosphorylation and dephosphorylation in a manner modulated by the accessory proteins KaiA and KaiB (*6*–*9*), and (ii) a transcriptional-translational feedback regulation (TTR) circuit in which the activity of the *kaiBC* promoter is under circadian control (*10*, *11*). The general architecture of coupled PTR and TTR loops is shared by circadian circuits in many species (*1*, *12*, *13*).

The role of the TTR and PTR in establishing and stabilizing circadian oscillations has been previously studied both experimentally (*9*, *14*–*17*) and theoretically (*18*). The PTR is required for circadian rhythms; abrogation of this circuit results in damped oscillations at the population level (*9*). However, the persistence of these oscillations is a subject of debate (*9*, *14*). By contrast, the TTR appears to be dispensable under some conditions (*15*, *16*). The PTR circuit alone can generate remarkably stable oscillations in vitro in a reconstituted system (*17*). Similarly, in vivo circadian oscillations are stable in dark conditions, where transcription is repressed and cells are not growing (*6*, *19*). Theoretical work has suggested that the TTR may be involved in generating robust circadian rhythms during growth (*18*).

To address the role of the TTR and PTR circuits in vivo in growing cells, we initially constructed two strains (Fig. 1A): (i) a wild-type strain in which both the TTR and PTR circuits are intact, and (ii) a PTR-only strain in which the TTR circuit was abrogated by making expression of the *kaiBC* operon constitutive and at a level similar to the mean expression of *kaiBC* in the wild-type strain (fig. S1). [A strain in which *kaiBC* expression

[1]Howard Hughes Medical Institute, Faculty of Arts and Sciences Center for Systems Biology, Department of Molecular and Cellular Biology and Department of Chemistry and Chemical Biology, Harvard University, Cambridge, MA 02138, USA. [2]Department of Chemistry and Chemical Biology, Harvard University, Cambridge, MA 02138, USA. [3]Department of Physics, Harvard University, Cambridge, MA 02138, USA.

*These authors contributed equally to this work.
†Corresponding author. E-mail: erin_oshea@harvard.edu

is under the control of an inducible promoter was previously characterized but is not a true PTR-only strain; we and others observed residual circadian dependence of *kaiBC* expression in this strain (fig. S1) (*11*, *20*).] We monitored the state of the clock by measuring fluorescence derived from expression of a gene encoding yellow fluorescent protein (YFP) under the control of the *kaiBC* promoter (*21*, *22*). YFP intensity reflects the abundance of the phosphorylated form of KaiC that is active in promoting circadian transcription (*21*).

We measured circadian oscillations over a wide range of growth rates in constant conditions with control of light and composition of the medium by means of a microfluidics device that limits its cellular crowding and replenishes spent nutrient buffer (Fig. 1B and fig. S2), permitting long-duration measurements in a chemostatic environment (*23*). After 2 days of entrainment in a test tube to generate a population of cells oscillating with the same phase, we loaded cells into this device and used automated methods to collect phase contrast (Fig. 1C) and fluorescence images (Fig. 1D) every 20 min for 5 days.

The population-averaged YFP fluorescence (fig. S3), as well as the signal in individual wild-type cell lineages (Fig. 2A), oscillated with circadian periodicity throughout the duration of the measurement. Moreover, a polar plot of the amplitude and phase for each cell lineage confirmed that the initial synchronization of this population, produced by entrainment, persisted throughout the 5-day measurement (Fig. 2B). The PTR-only strain also showed clear circadian oscillations for the population average (fig. S3) and for individual cells (Fig. 2C). After 1 day in constant light conditions, the variation in phase and amplitude within individual PTR-only cell lineages was comparable to that observed for the wild-type strain; however, after 4 days, the variation in the phase of these oscillations between individual PTR-only cell lineages increased (Fig. 2D). Thus, without the TTR circuit, the ability of the PTR-only strain to maintain the phase established by the original entrainment decreases and cell populations lose synchrony.

To quantify the phase stability as a function of time, we calculated the synchronization index (SI) (*24*). This index is based on the Shannon entropy of the phase distribution (see supplementary text) and varies from one for a completely synchronized population—where all cells oscillate with the same phase—to zero for an unsynchronized population, in which cells oscillate with random phases. The SI for the wild-type strain started high and decreased ~25% over the 5-day measurement (Fig. 2E). The SI for the PTR-only strain started at approximately the same value as the wild-type strain, indicating that disruption of the TTR circuit does not affect entrainment of this strain to light and dark cycles. However, once these external cues were removed, the population of PTR-only cells quickly desynchronized, dropping roughly 70% in SI over 5 days (Fig. 2E). The PTR-only strain

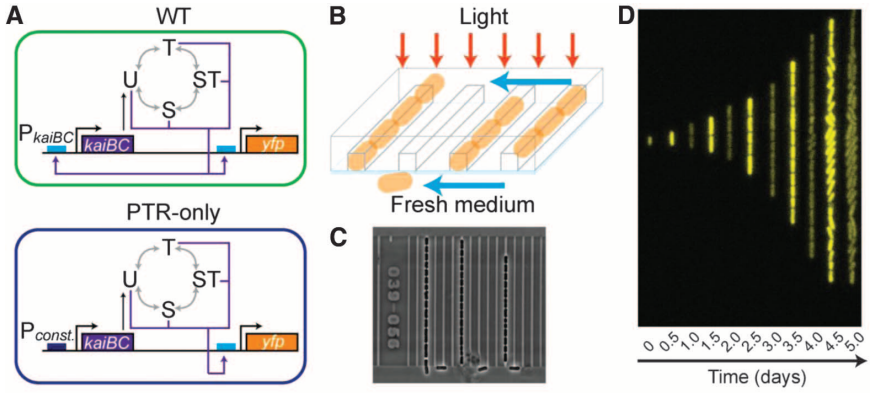

Fig. 1. Long-term measurement of circadian oscillations in *S. elongatus*. (**A**) Genetic circuit diagrams of the wild-type strain (WT) and the PTR-only strain. KaiC has two phosphorylation sites and transits through four different phosphorylated forms in the PTR circuit during the circadian cycle: unphosphorylated (U-KaiC, represented by 'U'); phosphorylated only on Thr^{432} (T-KaiC, 'T'); phosphorylated on both Ser^{431} and Thr^{432} (ST-KaiC, 'ST'); and phosphorylated only on Ser^{431} (S-KaiC, 'S') (*7*, *8*). In the WT strain, both the KaiC PTR (gray arrows) and TTR (purple arrows) circuits are intact. In the PTR-only strain, the *kaiBC* operon is under the control of a constitutive promoter, abrogating transcriptional regulation. In both strains, a YFP reporter is under the control of the *kaiBC* promoter, whose activity is regulated by the phosphorylation state of KaiC (the PTR). (**B**) Schematic of growth in the patterned agarose microenvironment. Cells are trapped at the interface between a coverglass and a patterned agarose gel, and a chemostatic environment is maintained by a flow of fresh medium and constant light. (**C**) *S. elongatus* cells growing in the microfluidics device imaged using phase-contrast microscopy. (**D**) Fluorescence image collage of subsequent frames of a time-lapse movie of WT cells.

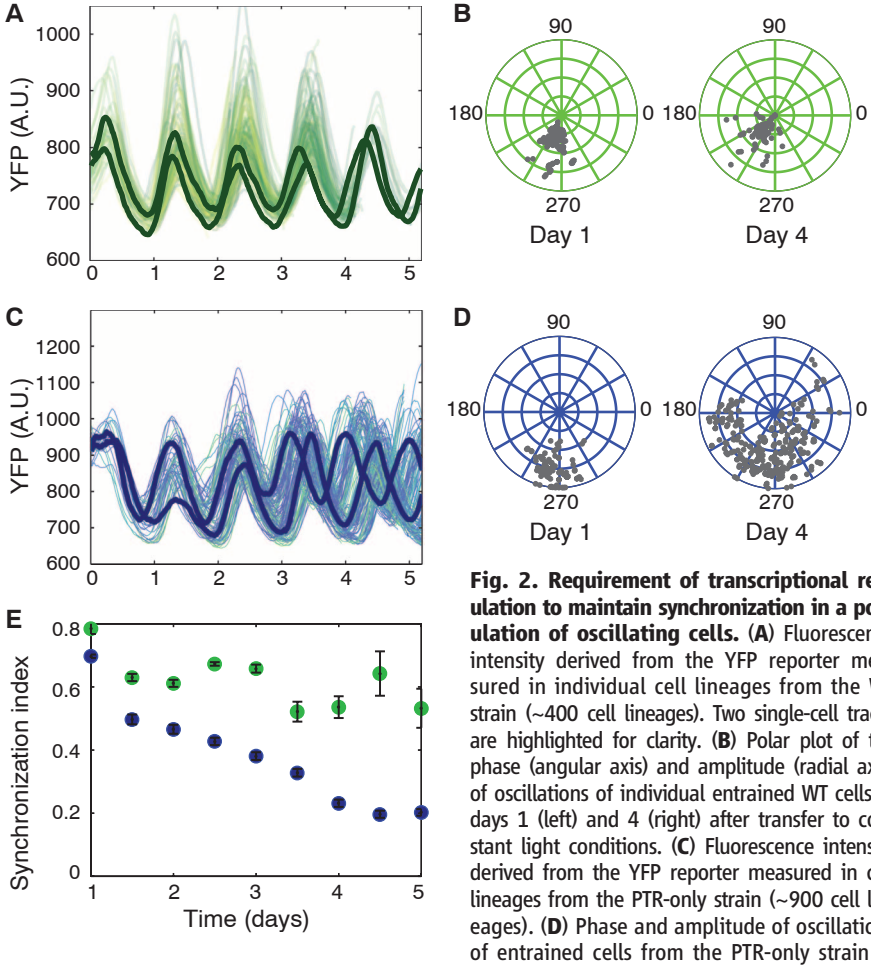

Fig. 2. Requirement of transcriptional regulation to maintain synchronization in a population of oscillating cells. (**A**) Fluorescence intensity derived from the YFP reporter measured in individual cell lineages from the WT strain (~400 cell lineages). Two single-cell traces are highlighted for clarity. (**B**) Polar plot of the phase (angular axis) and amplitude (radial axis) of oscillations of individual entrained WT cells at days 1 (left) and 4 (right) after transfer to constant light conditions. (**C**) Fluorescence intensity derived from the YFP reporter measured in cell lineages from the PTR-only strain (~900 cell lineages). (**D**) Phase and amplitude of oscillations of entrained cells from the PTR-only strain at days 1 and 4 after transfer to constant light conditions. (**E**) Synchronization index for the ensemble of cells as a function of time for the WT (green) and PTR-only (blue) strains (see supplementary text for details). Error bars are derived by the bootstrap method.

desynchronized more quickly when it was growing faster (one division every 14 to 16 hours; fig. S4H) than the circadian period than when it was growing more slowly (one division every 72 hours; Fig. 2 and fig. S4G). Thus, the TTR had a more important role in stabilizing circadian oscillations for cells with faster growth rates, in qualitative agreement with the predictions of the model we describe below (fig. S5) as well as a previous modeling study (*18*).

To explore the properties of the TTR circuit, we quantified the dynamics of a mutant KaiC$^{S431E/T432E}$ strain lacking the PTR but containing an intact TTR circuit (the "TTR-only strain," in which the potential for feedback regulation of *kaiBC* expression exists) (Fig. 3A and fig. S6) (*9*, *14*). This strain showed an initial decrease in fluorescence intensity after transfer to constant light conditions that then increased and stabilized on the first day to an average expression level around which individual cells fluctuated (Fig. 3B). Similar behavior was observed for faster growth rate (fig. S7). The initial dip appeared to be set by the entrainment protocol (fig. S6D) and was not affected by the transfer of cells to the microfluidics device.

To determine which strains exhibit circadian oscillations, we calculated the average of the power spectrum of the fluorescence intensity of individual cell lineages (Fig. 3C). The wild-type and PTR-only strains had nearly identical power spectra with a prominent peak at the expected 1-day period. A comparable peak was not present for the TTR-only strain, confirming that there were no circadian oscillations in this strain. This result is consistent with population studies that reported damped oscillations of a clock transcriptional reporter in the KaiC$^{S431E/T432E}$ strain (*9*). Thus, the role of the PTR circuit is to establish the oscillations and the role of the TTR circuit is to stabilize these oscillations in growing cells.

To explore the interplay of the PTR and TTR circuits, we created a mathematical model of in vivo circadian oscillations in *S. elongatus* that consisted of a PTR pacemaker and a TTR controller (Fig. 3D). The PTR portion of the model was based on a model of the in vitro oscillator (*7*) with addition of terms to account for loss of protein due to degradation and dilution (*25*). The TTR portion of the model consists of a simple negative feedback loop in which the clock protein KaiC represses its own mRNA synthesis. We performed least-squares fitting to our experimental data from the TTR-only strain to derive model parameters that constrain the negative feedback describing the TTR circuit and found that the experimentally observed dynamics of the reporter in the TTR-only strain could be accurately represented by this simple model (Fig. 3E). This model constrained by parameters determined from experiments (table S1) also reproduced the sustained oscillations observed in the population average data for the wild-type and PTR-only strains (Fig. 4A and fig. S3).

To determine whether our model could recapitulate circadian oscillations of the wild-type versus PTR-only strains in individual cell lineages, we performed stochastic simulations of the model using parameters determined from experiments (table S1) (*26*). We found that the wild-type model produces circadian oscillations (Fig. 4B) that desynchronize only weakly with time (Fig. 4C), although not as weakly as observed experimentally, presumably because of simplifications in the model (such as treating KaiC as a monomer rather than a hexamer). The PTR-only model, however, produces circadian oscillations (Fig. 4D) that desynchronize far more rapidly than the wild-type model and that desynchronize more quickly with increased growth rate (Fig. 4, E and F, and fig. S5), as observed experimentally. Repression of *kaiBC* transcription by U-KaiC and S-KaiC (see legend to Fig. 1 for details of the PTR circuit) creates a peak of *kaiBC* mRNA prior to the peak of U-KaiC in the PTR circuit. As a result, newly synthesized U-KaiC accumulates coincidentally with the rise of U-KaiC from the PTR cycle, and this synchronization of new and existing U-KaiC enhances the stability of the PTR cycle, increasing the robustness of the oscillator (*18*).

To characterize the extent to which the TTR circuit enhances robustness of the circadian oscillator to variability in clock components and

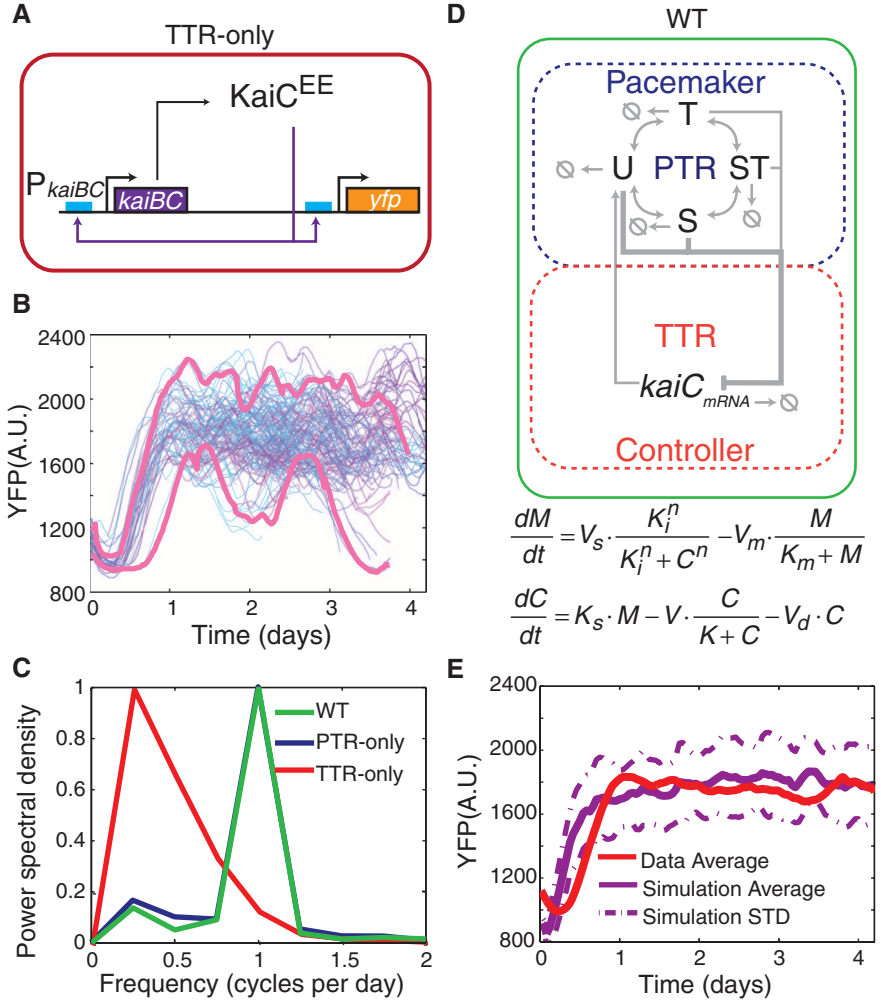

Fig. 3. Insufficiency of transcriptional feedback in the absence of a PTR circuit to generate circadian oscillations. (**A**) Genetic circuit diagram of the TTR-only strain. (**B**) Fluorescence intensity derived from the YFP reporter measured in individual entrained cell lineages of the TTR-only strain (~400 cell lineages). Two single-cell traces are randomly selected and highlighted in pink. Cells are dividing once every 24 hours. (**C**) The average of power spectra of single-cell fluorescence traces from the WT strain (green), PTR-only strain (blue), and TTR-only strain (red). (**D**) Diagram of the model of the WT circuit. Oscillations are generated by the PTR circuit (pacemaker in the blue dashed box), and abundance of newly made KaiC is controlled by the TTR circuit (controller in the red dashed box). "Ø" represents degradation. Two equations describe the controller dynamics as negative feedback, in which KaiC (C) regulates its own mRNA (M) synthesis in a Hill repression function (see supplementary text for details). (**E**) The average YFP expression (red solid line) for the ensemble of cells from the TTR-only strain. The purple solid line shows the average of the stochastic simulated traces generated from the equations in (D); the purple dashed lines indicate SD of the simulated traces.

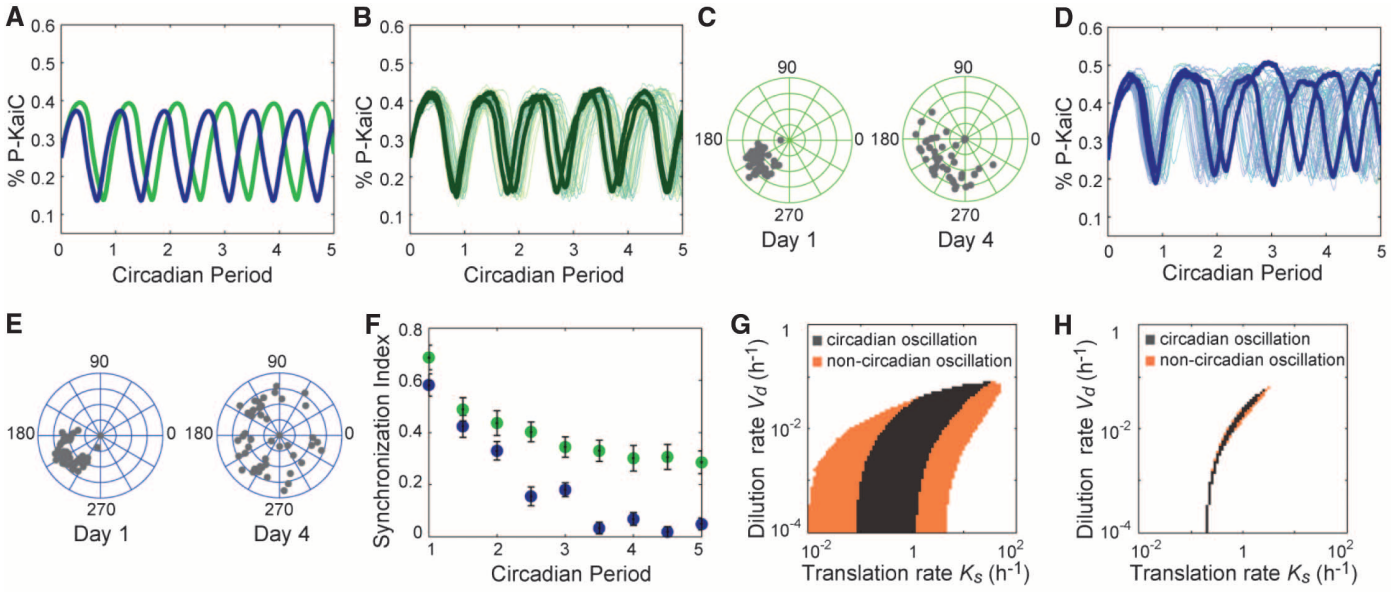

Fig. 4. Requirement of transcriptional feedback for robustness of in vivo oscillations. (**A**) Deterministic simulations of circadian oscillation of KaiC phosphorylation for the WT (green) and PTR-only (blue) circuits. The simulated period of the PTR-only strain is 6% shorter than that of the WT strain. (**B**) Stochastic simulated traces for the WT strain. Two of the 100 displayed traces were randomly selected and highlighted. (**C**) Phase versus amplitude plot of simulated traces for the WT strain at days 1 and 4. (**D**) Stochastic simulated traces (100 traces) of circadian oscillation of KaiC phosphorylation for the PTR-only strain. (**E**) Phase versus amplitude plots for simulations of the PTR-only strain. (**F**) Synchronization index for the stochastic simulated traces as a function of time for the WT (green) and PTR-only (blue) strains. (**G** and **H**) Sensitivity analysis of the oscillation period. Models of the WT (G) and PTR-only (H) systems were numerically solved for dilution and translation rates simultaneously varied over four orders of magnitude. Solutions with periods ±5 hours around the circadian period of the model output were classified as circadian (black), and other solutions yielding stable oscillations outside this range were denoted noncircadian (orange). We selected ±5 hours because the same relative range of periods is observed in the measured WT system power spectrum in Fig. 3C.

cellular growth, we performed a systematic sensitivity analysis of the wild-type and PTR-only models. We varied the values of parameters common to both the wild-type and PTR-only models, numerically integrated the wild-type and PTR-only model differential equations, and analyzed the power spectra of the resulting time trajectories to detect circadian oscillations. We find that the volume of parameter space that supports circadian oscillations in the wild-type system (Fig. 4G) is far larger than that of the PTR-only model (Fig. 4H). Furthermore, within the space of parameters supporting circadian oscillations, the wild-type system experiences much smaller changes in period upon parameter variation than does the PTR-only system (Fig. 4, G and H, and fig. S8) (see supplementary text). Thus, the TTR circuit is able to buffer the circadian oscillator against stochastic fluctuations in clock components, and also against sustained changes in parameters such as the cellular growth rate and KaiC translation and degradation rates, all of which cause profound changes in the PTR-only system when varied (fig. S8).

Our findings show that the PTR can generate oscillations in vivo in the absence of TTR feedback. However, without TTR feedback, populations of cells lose synchrony because of phase drift of individual oscillators. Coupling of the PTR pacemaker to the TTR controller generates robustness—insensitivity of period and phase to changes in parameters—that enables the clock to maintain accurate oscillations in the absence of external cues for long durations and that explains the remarkable stability of the cyanobacterial clock. This architecture may represent a general solution used in other circadian circuits.

References and Notes

1. J. C. Dunlap, J. J. Loros, P. J. Decoursey, Eds., *Chronobiology: Biological Timekeeping* (Sinauer, Sunderland, MA, 2004).
2. S. L. Harmer, S. Panda, S. A. Kay, *Annu. Rev. Cell Dev. Biol.* **17**, 215 (2001).
3. J. C. Dunlap, *Cell* **96**, 271 (1999).
4. I. Mihalcescu, W. H. Hsing, S. Leibler, *Nature* **430**, 81 (2004).
5. M. Amdaoud, M. Vallade, C. Weiss-Schaber, I. Mihalcescu, *Proc. Natl. Acad. Sci. U.S.A.* **104**, 7051 (2007).
6. J. Tomita, M. Nakajima, T. Kondo, H. Iwasaki, *Science* **307**, 251 (2005).
7. M. J. Rust, J. S. Markson, W. S. Lane, D. S. Fisher, E. K. O'Shea, *Science* **318**, 809 (2007).
8. J. S. Markson, E. K. O'Shea, *FEBS Lett.* **583**, 3938 (2009).
9. X. M. Qin, M. Byrne, Y. Xu, T. Mori, C. H. Johnson, *PLoS Biol.* **8**, e1000394 (2010).
10. M. Ishiura *et al.*, *Science* **281**, 1519 (1998).
11. Y. Nakahira *et al.*, *Proc. Natl. Acad. Sci. U.S.A.* **101**, 881 (2004).
12. M. W. Young, S. A. Kay, *Nat. Rev. Genet.* **2**, 702 (2001).
13. M. Gallego, D. M. Virshup, *Nat. Rev. Mol. Cell Biol.* **8**, 139 (2007).
14. Y. Kitayama, T. Nishiwaki, K. Terauchi, T. Kondo, *Genes Dev.* **22**, 1513 (2008).
15. J. S. O'Neill, A. B. Reddy, *Nature* **469**, 498 (2011).
16. J. S. O'Neill *et al.*, *Nature* **469**, 554 (2011).
17. M. Nakajima *et al.*, *Science* **308**, 414 (2005).
18. D. Zwicker, D. K. Lubensky, P. R. ten Wolde, *Proc. Natl. Acad. Sci. U.S.A.* **107**, 22540 (2010).
19. N. Hosokawa *et al.*, *Proc. Natl. Acad. Sci. U.S.A.* **108**, 15396 (2011).
20. Y. Xu, T. Mori, C. H. Johnson, *EMBO J.* **22**, 2117 (2003).
21. J. R. Chabot, J. M. Pedraza, P. Luitel, A. van Oudenaarden, *Nature* **450**, 1249 (2007).
22. Q. Yang, B. F. Pando, G. Dong, S. S. Golden, A. van Oudenaarden, *Science* **327**, 1522 (2010).
23. J. R. Moffitt, J. B. Lee, P. Cluzel, *Lab Chip* **12**, 1487 (2012).
24. P. Tass *et al.*, *Phys. Rev. Lett.* **81**, 3291 (1998).
25. D. Gonze, J. Halloy, A. Goldbeter, *Proc. Natl. Acad. Sci. U.S.A.* **99**, 673 (2002).
26. D. T. Gillespie, *J. Phys. Chem.* **81**, 2340 (1977).

Acknowledgments: We thank P. Cluzel for the development of the microfluidics platform upon which the device used in this paper is based (funded via National Institute of Allergy and Infections Diseases award 1R21AI094363-01A1); B. Goetze and J. Wailes for assistance with microscopy; D. Zwicker, P. R. ten Wolde, and A. Subramaniam for stochastic simulation; J. Markson, A. Gutu, V. Vijayan, and A. Puszynska for strain construction and Western blotting; P. Cluzel, D. Gonze, and P. de Buyl for helpful discussion; and B. Stern, J. Markson, V. Vijayan, A. Rizvi, M. Rust, and A. Subramaniam for comments on the manuscript. Supported by the Helen Hay Whitney Postdoctoral Fellowship (J.R.M.), Fonds National de la Recherche Scientifique Belgium (postdoctoral researcher) (S.d.B.), Wallonie-Bruxelles International (S.d.B.), Wallonie-Bruxelles International (S.d.B.), and the Howard Hughes Medical Institute (E.K.O.).

Supplementary Materials

www.sciencemag.org/cgi/content/full/340/6133/737/DC1
Materials and Methods
Supplementary Text
Figs. S1 to S10
Table S1
References (*27*–*38*)

2 October 2012; accepted 13 March 2013
10.1126/science.1230996